Rheological Behavior of SAN/PC Blends Under Extremely High Shear Rate

HIDEROH TAKAHASHI, TAKAAKI MATSUOKA, TAKASHI OHTA, KENZO FUKUMORI, TOSHIO KURAUCHI, and OSAMI KAMIGAITO, *Toyota Central Research and Development Laboratories, Inc., Nagakute-cho, Aichi-gun, Aichi-ken, 480-11, Japan*

Synopsis

Extremely high shear rate processing was applied to the compound system of acrylonitrile-styrene copolymer/polycarbonate (SAN/PC). The viscosity was measured against the shear rate up to 10^7 s^{-1}.

The first non-Newtonian region, the second Newtonian region and second non-Newtonian region were observed in the compound system. The occurrence of these regions are very similar to those in the parent polymers, SAN and PC. For the calculation of the viscosity-shear rate curve, a concentric multilayer model was proposed. It gives good agreement between the calculated value and the measured one. A new mechanism for the occurrence of the non-Newtonian, second Newtonian, and second non-Newtonian regions was proposed. Nuclear spin–spin relaxation time measured on SAN, T_2, seems to be consistent with the consideration that the occurrence of non-Newtonian region, second Newtonian region, and second non-Newtonian region are caused, respectively, by the disentanglement, near saturation of disentanglement associated with snapping of macromolecules, and reentanglement through recoiling of snapped macromolecules, and further snapping of the macromolecules, which is inconsistent with the proposed explanation.

INTRODUCTION

Extremely high shear rate rheometer was developed and applied to some single polymer systems, polystyrene, high-density polyethylene, ultra-high-molecular-weight polyethylene, acrylonitrile-styrene copolymer (SAN), polycarbonate (PC), polypropylene, and polyamide-6,6.[1]

Non-Newtonian region up to about 10^6 s^{-1}, and second Newtonian region from about 10^6–10^7 s^{-1} followed by the second non-Newtonian region were found in these polymers.

There is also interest in compound systems or blends, since compound polymer systems are very useful and some new or improved properties of the polymer systems exposed to extremely high shear rate can be expected. The first practical application of this processing to a compound polymer system involved an SAN and PC compound system which was exposed to extremely high shear rates up to about 10^7 s^{-1}. The rheology of the molten compound polymers was then studied.

Some probable mechanisms of occurrence of the first non-Newtonian region, the second Newtonian region, and the second non-Newtonian region are proposed, but its experimental examination is incomplete. Difficulty in measuring the entanglement density is responsible for the lack of experimental

Journal of Applied Polymer Science, Vol. 37, 1837–1853 (1989)
 CCC 0021-8995/89/071837-17$04.00

study of the mechanisms. Recently nuclear spin–spin relaxation time, T_2, has been suggested to be closely related to the degree of molecular entanglement.[2] In the present study, T_2 analysis was applied to examine the proposed mechanisms. In addition, analysis of nuclear spin–spin relaxation time, T_2, suggested a close relation would be examined in the system.

EXPERIMENTS

Figure 1 is an outline of the specially designed capillary rheometer. The details of the rheometer are described in a previous report.[1] The capillary, 0.5 mm diameter; 10 mm length, was used for the rheological measurements.

Pressures and velocity were recorded against the plunger position on an X-Y recorder.

The shear stress at the capillary wall, τ_w, is given by the following equation,

$$\tau_w = \frac{\Delta PR}{2L} \tag{1}$$

where ΔP is a pressure drop along the die, R and L are the radius and the length of the capillary, respectively.

The apparent shear rate, $\dot{\gamma}_a$, is given by the following equation,

$$\dot{\gamma}_a = \frac{4Q}{\pi R^3} \tag{2}$$

where Q is the volumetric flow rate, given from velocity of the plunger. The apparent viscosity, η_a, is defined as follows,

$$\eta_a = \frac{\tau_w}{\dot{\gamma}_a} \tag{3}$$

The materials are commercially available: SAN (Sanrex SAN-H, Mitsubishi Monsant Chemical) and PC (Iupilon S-3000, Mitsubishi Gas Chemical). The composition of the blends was varied from 30/70 to 70/30 in weight ratio. Blends were prepared in pellet form using a conventional twin-screw extruder

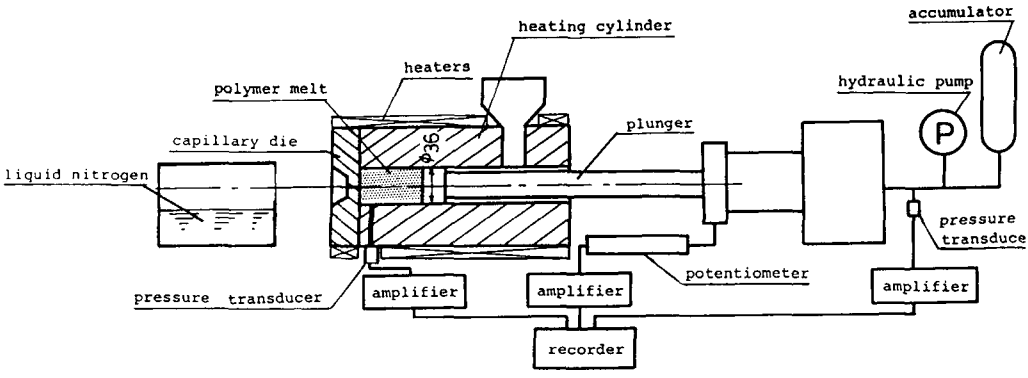

Fig. 1. Outline of the specially designed capillary rheometer.

at the temperature of 230°C. The stock temperature was controlled to be 280°C for most of the study described in this article.

Viscosity of the blends was measured against the shear rate up to 10^7 s^{-1}.

SAN was extruded into liquid nitrogen at the wide range of the shear rate up to 10^7 s^{-1} and cooled as soon as possible to quench entangled macromolecules under the various extruding conditions.

Nuclear spin–spin relaxation time, T_2, was measured on the SAN extrudates to estimate the degree of interaction, which is related to entanglement density, by using pulsed nuclear magnetic resonance (NMR) method. JEOL-FSE-60Q pulsed nulcear magnetic resonance spectrometer (14 kGauss, resonance frequency of 60 MHz, ^1H) was used.

The T_2 signal for the rubbery state of polymers is given by the following equation.[3]

$$M(t) = \sum_i Mi \exp\left(-\frac{t}{T_2 i}\right) \tag{4}$$

where Mi is the amplitude of the i-th component (proportional to the fraction of protons), and $T_2 i$ is spin–spin relaxation time T_2 of the i-th component. $T_2 i$ and the fractional component of $T_2 i$, which is defined as $Mi/\sum_i Mi$, are calculated by nonlinear least-squares method.

The solving rate was measured to estimate the degree of entanglement of the extruded SAN.

For measuring the solving rate of the extruded SAN in the mixture of tetrahydrofuran (THF) 80% and cyclohexane 20%, the dissolved SAN in the solvent at a given time was measured. In this experiment, small particles ~ 0.1 mm diameter were prepared and 0.05 g of the particles was put into the solvent at 23°C. After 4 minutes, the solution was filtered and the molecular weight distribution of the dissolved SAN was measured by gel-permeation chromatography (GPC). The amount of dissolved SAN was calculated from the GPC data.

X-ray analysis was tried to study the molecular orientation in the extruded macromolecules, using CuKα.

RESULTS AND DISCUSSION

The apparent viscosity of the blends is plotted against apparent shear rate in Figure 2.

As the viscosity of PC is very large at 280°C, the flow curve could not be determined at shear rates higher than 1×10^6 s^{-1}. A linearly decreasing flow curve was observed in the region.

A second Newtonian region, in which the apparent viscosity is constant against shear rate, was observed for SAN in the high shear rate region ($> 2.7 \times 10^6$ s^{-1}). An increase in the apparent viscosity was found at the apparent shear rate of about 4×10^6 s^{-1}, above which the second non-Newtonian region appears. Near the shear rate corresponding to the end of the plateau region, the measured viscosity scattered slightly. The flow near the shear rate seems to be slightly unstable.

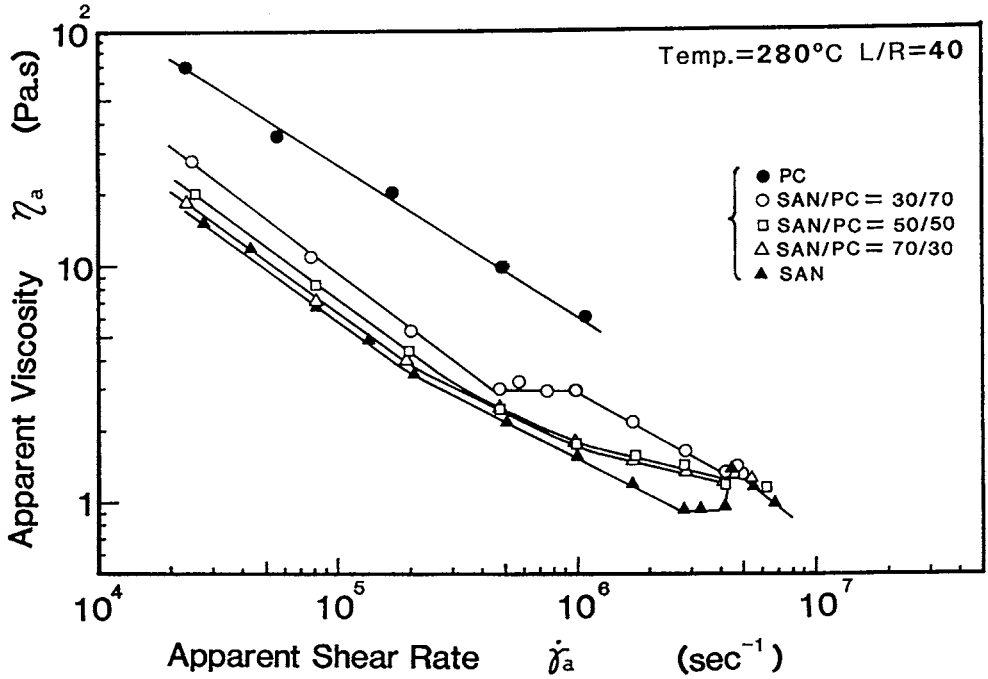

Fig. 2. Plot of apparent viscosity η_a vs. apparent shear rate $\dot{\gamma}_a$ for SAN/PC blend. ● PC; ○, SAN 30/PC 70; □, SAN 50/PC 50; △, SAN 70/PC 30; ▲, SAN. Temperature 280°C, L/R = 40.

Concerning the compound systems, all three regions occur at similar rates. The second Newtonian region begins and ends at shear rates of 5.0×10^5 s^{-1} and 1.0×10^6 s^{-1}, respectively, for SAN 30% PC 70% system. For SAN 50% PC 50% and SAN 70% PC 30% systems, the flow curves have no evident plateau region. But, they do have small gradient regions between the shear rate of about 10^6 s^{-1} and that of about 5.0×10^6 s^{-1}. This region is thought to correspond to the second Newtonian region, which should be called as pseudo-Newtonian region. The beginning of the pseudo-Newtonian region is determined from the intersecting point of the curves extrapolated from the first non-Newtonian region and from the shear rate region of 1.0×10^6 s^{-1} to 2.0×10^6 s^{-1}. The beginning points are 1.3×10^6 s^{-1} for SAN 50% PC 50% and 1.8×10^6 s^{-1} for SAN 70% PC 30%. The beginning point is considered to correspond substantially to that of the second Newtonian region as mentioned.

There is a slight but abrupt increase in viscosity at the shear rate of 4.5×10^6 s^{-1} for SAN 50% PC 50% and SAN 70% PC 30 % systems. The shear rate of 4.5×10^6 s^{-1} is nearly the same as that in the single system, SAN, at the same temperature.

The occurrence of the first non-Newtonian region is thought to be attributed to the decrease of entanglement density resulting from the disentanglement caused by shear flow, as studied by Soong and Shen.[4] As the shear rate is increased further, the number of entangled macromolecules will become very small, at least near the capillary wall. Further disentanglement occurs in this region but the rate of decrease against the increase of shear rate would

become very small. In this region the plateau takes place, and the macromolecules will be stretched close to their full length.

As the shear rate is further increased, the fully or near fully stretched macromolecules will snap in two. The snapped macromolecules tend to recoil under the influence of the strain energy stored under the shear at the very moment of snapping. The recoiling macromolecules reentangle the neighboring macromolecules, creating new entanglement. The snapping results in the decrease of viscosity through the decrease of the molecular weight of the macromolecules. The creation of new entanglement results in the increase of viscosity. The change of viscosity under the influences of the contrary effects of the decrease and the increase is thought to depend on the molecular weight and structure of the macromolecules. In SAN and the composite systems studied in this experiment, the increase of viscosity through the creation of new entanglement would be superior to the decrease resulting in the abrupt increase in the viscosity at the end of the plateau region. This snapping is thought to occur throughout the plateau region, although the change of viscosity is unremarkable.

As the shear rate is increased further, the entangled macromolecules are more frequently disentangled by the increased shear flow and snapping of the stretched macromolecules is increased. This tends to decrease the viscosity, overcoming the tendency toward increased viscosity through creating new entanglement. This would account for the occurrence of the second non-Newtonian region.

The weight-averaged molecular weight for extruded SAN is shown in Figure 3.

The molecular weight is nearly constant below the shear rate of 10^6 s^{-1}. It decreases remarkably above the shear rate of 2×10^6 s^{-1}, where the second Newtonian region or plateau region and the second non-Newtonian region exist. This result supports the above explanation for the occurrence of the

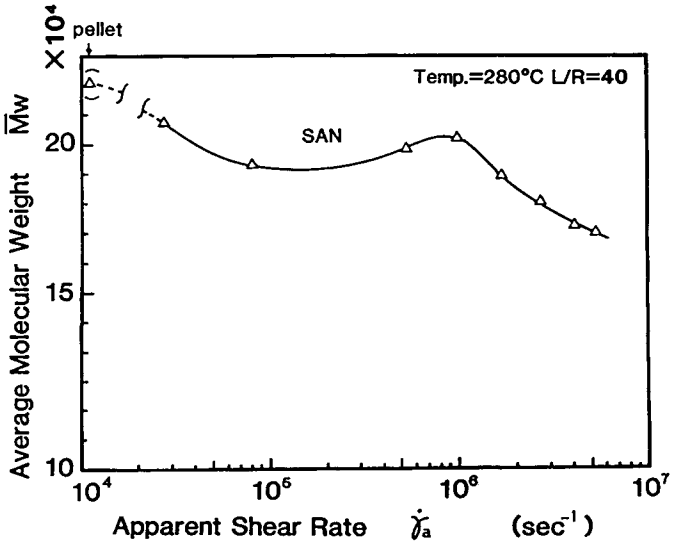

Fig. 3. Weight-average molecular weight $\overline{M}_w$ of extruded SAN. Temperature 280°C; L/R = 40.

suggested snapping of stretched macromolecules in the plateau region, that at the shear rate of 4×10^6 s^{-1}, and that above the plateau region or the second non-Newtonian region.

Spin–spin relaxation time, T_2, of SAN is shown in Figure 4. T_2 is divided into two components, the shorter T_2 and the longer T_2 in temperature range from 140°C to 165°C. Outside the range, two T_2 turn in one component. The shorter T_2 is considered to be related to the interaction depending on cross-linking and molecular entanglement and the longer one to the micro-Brownian movement of macromolecules.[2,5]

Fractional component of the shorter T_2 is plotted against the shear rate under which SAN was extruded in Figure 5. The T_2 component decreases with the shear rate to about 63%, then increases above the shear rate of 2×10^6 s^{-1}, followed by second decrease. The increase in the component at about 64.7% corresponds approximately to the beginning of the plateau region in $\eta_a \sim \dot{\gamma}_a$ curve.

The decreased value of the component of 64.3% occurs in the specimen exposed to the highest shear rate of 7×10^6 s^{-1}, which lies in the second non-Newtonian region. According to Charlesby et al.,[2] the T_2 component is closely related to the presence of entanglement in macromolecules.

Following this analysis, the variation of the T_2 component with the shear rate shows that the entanglement density first decreases with shear rate, which is consistent with the conventional interpretation that the decrease of viscosity with the shear rate is caused by the decrease of the entanglement density in the non-Newtonian region. This seems, in turn, to support the analysis made by Charlesby et al. as correct also for the present polymers. The increase of the T_2 component near the beginning of the plateau region means that entanglement after the snapping of the macromolecules takes place there,

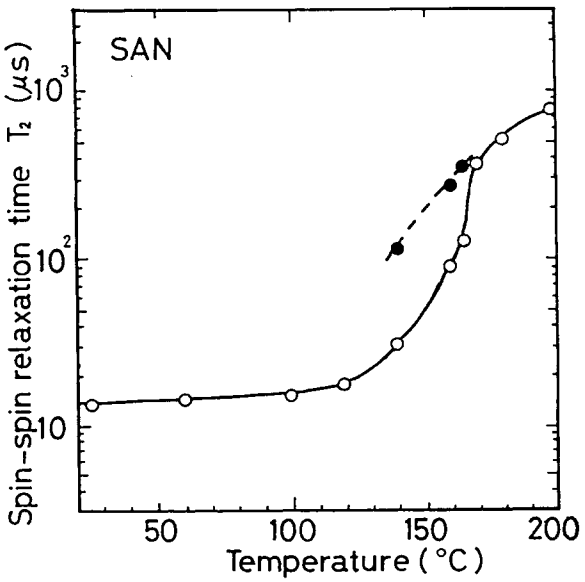

Fig. 4. Plot of spin–spin relaxation time, T_2, of SAN against temperature.

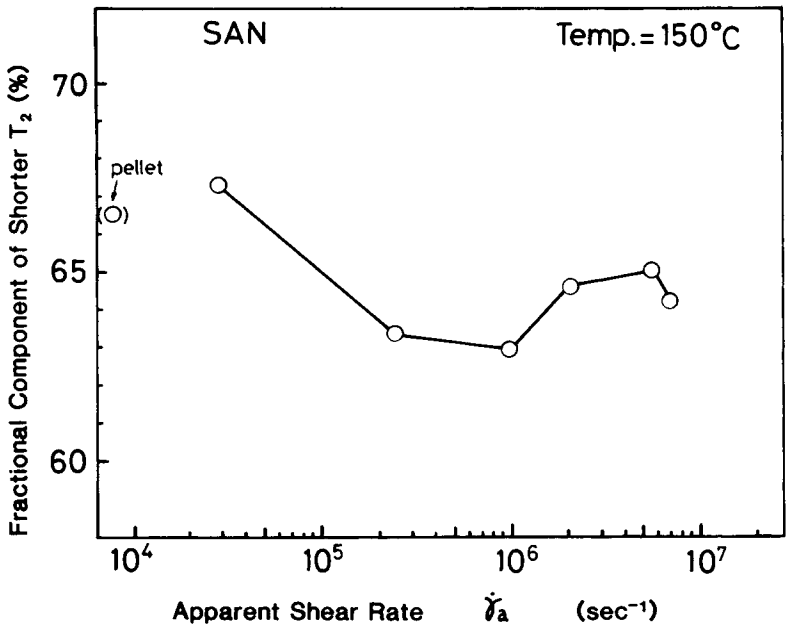

Fig. 5. Plot of fractional component of the shorter T_2 of extruded SAN against the shear rate. Temperature 150°C.

which is consistent with the above explanation for the occurrence of the plateau region and the increased viscosity. The decrease at the shear rate of 7×10^6 s^{-1} shows that the entanglement density decreases there, implying that further snapping of macromolecules occurs frequently, consistent with the explanation and the results concerning the molecular weight variation.

The T_2 component with the annealed specimens is plotted against the shear rate in Figure 6. It decreases gradually with the rate, and the fractional value itself increases nearly to the original value from that, with the exceptions of the largest value (67%) and the smallest value (64%). The increase in the component means that the disentangled macromolecules are reentangled by thermal agitation in annealing. This shows that the construction of each macromolecule is not greatly modified from its original one, since the T_2 component will not be nearly the same as the original value if the construction is significantly modified. In this polymer system, then, the decrease of T_2 component is thought to be caused mainly by the decrease of entanglement density, associated with little change in the construction. This result is consistent with the explanation for the occurrence of non-Newtonian and the plateau region. The invariance of the value at the shear rate of 2.7×10^4 s^{-1} is interpreted to show that disentanglement under the shear does not occur so frequently, giving rare recovery of entanglement. The invariance at the highest shear rate shows that the decreased viscosity is caused mainly through the snapping of the macromolecules, which is consistent again with the previously mentioned explanation and results.

Figure 7 plots the amount of dissolved SAN in solvent against the shear rate under which the specimen was extruded. The amount is nearly the same

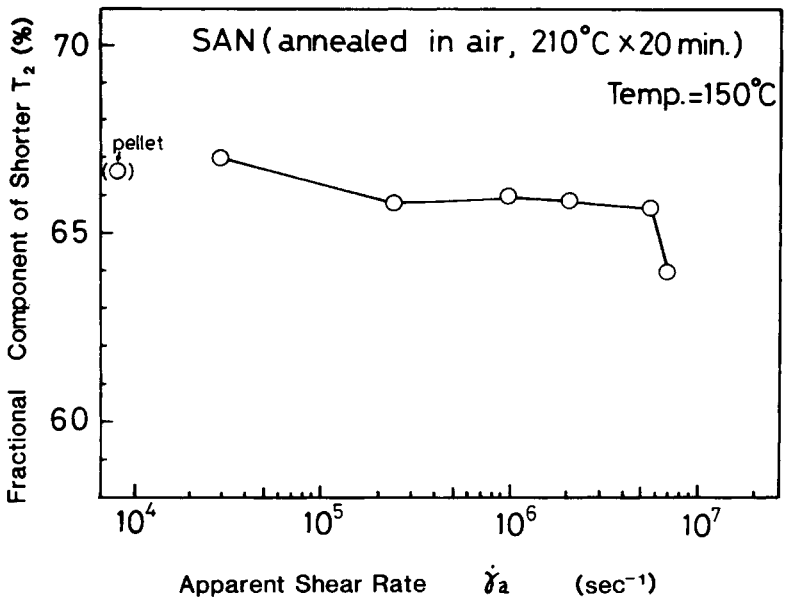

Fig. 6. Plot of fractional component of the shorter T_2 of extruded SAN annealed in air (210°C × 20 min) against the shear rate. Temperature 150°C.

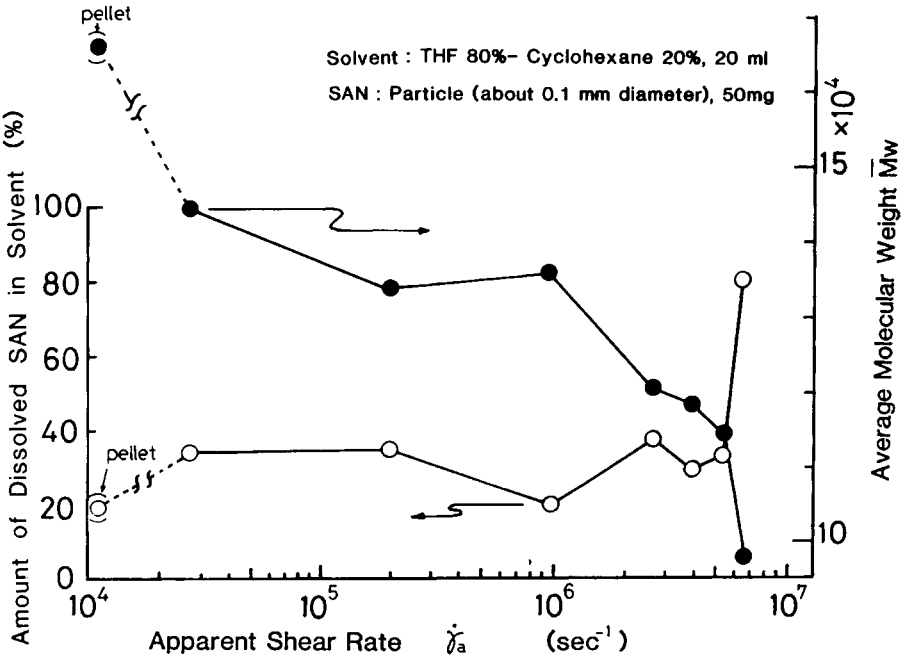

Fig. 7. Plot of amount of dissolved SAN in solvent (THF 80%-cyclohexane 20%) against shear rate.

against the shear rate. It increases at the shear rate at which the viscosity decreases again.

The weight-averaged molecular weight of SAN dissolved in the solvent is also shown in Figure 7, as a function of the shear rate. It is nearly the same against the rate, and decreases at the rate where viscosity decreases again, corresponding to the increase of solving rate. Then, the increased solving rate is considered to be attributed to the decrease of the molecular weight. The solving rate measurement was not always suitable for estimating the degree of entanglement.

X-ray analysis showed no high orientation in the extruded macromolecules.

From these results, the microstructure of the macromolecules is interpreted to vary with shear rate as shown schematically in Figure 8.

The viscosity-shear rate relationship in the binary system will be understood by analyzing the flow in the experimental system. The binary system is composed of the dispersoid and the matrix [Fig. 9(a)].

The number of the dispersoid is given by the following equation.

$$n = \frac{\pi R_1^2 \omega_B}{\frac{4}{3}\pi\left(\frac{d}{2}\right)^3} \tag{5}$$

where d is a diameter of a dispersoid, R_1, radius of the capillary, ω_B, volumetric fraction of B component.

The flow in the actual binary system shown in Figure 9(a) looks too tedious to solve analytically. Therefore, a special model[6] which can be dealt with easily must be introduced. For this purpose, the model shown in Figure 9(b) was introduced.

It is a concentric multilayer composite of alternating layers of PC(A) and SAN(B). The volume ratio of each layer is selected so as to be the same as that of each material. Moreover, the area of the interface between the layers is selected so as to be the same as that between the dispersoids and matrix, in which the size of the dispersoid is assumed to be 1 μm.

One these assumptions, the number (N), the thickness (a, b) of the layers are given by the following.

$$N = \frac{6R_1\omega_B}{2d} \tag{6}$$

$$a = \frac{2R_1(1 - \omega_B)}{2(N + 1)} \tag{7}$$

$$b = \frac{d}{3} \tag{8}$$

The flow in the multilayer model is given as follows;

Using cylindrical coordinates, the z component of the equations of motion for tubular flow is written[7]

$$-\frac{\partial P}{\partial z} + \frac{1}{r}\frac{\partial}{\partial r}(r\tau_{rz}) = 0 \tag{9}$$

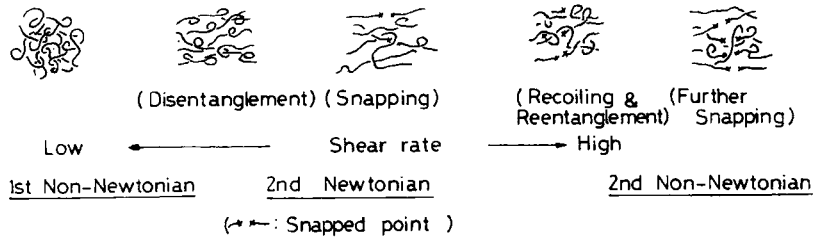

Fig. 8. Schematic drawing of microstructure variation of macromolecules with shear rate.

For the power-low fluid defined as

$$\tau_{rz} = K\left(\frac{\partial V_z}{\partial_r}\right)^n \tag{10}$$

or

$$\eta = K\left(\frac{\partial V_z}{\partial r}\right)^{n-1} \tag{11}$$

in which K and n are power-law constants, integrating Eq. (9) gives velocity profiles, $V_{A,i}$ and $V_{B,i}$, for phase A layer and phase B layer as follows.

$$V_{A,i} = \sum_{j=1}^{i-1} Z_{A,j}\left(R_{2j-1}^{1+\alpha_{A,j}} - R_{2j}^{1+\alpha_{A,j}}\right) + Z_{A,i}\left(R_{2i-1}^{1+\alpha_{A,i}} - r^{1+\alpha_{A,i}}\right)$$
$$+ \sum_{j=1}^{i-1} Z_{B,j}\left(R_{2j}^{1+\alpha_{B,j}} + R_{2j+1}^{1+\alpha_{B,j}}\right) \tag{12}$$

$$V_{B,i} = \sum_{j=1}^{i} Z_{A,j}\left(R_{2j-1}^{1+\alpha_{A,j}} - R_{2j}^{1+\alpha_{A,j}}\right) + \sum_{j=1}^{i-1} Z_{B,j}\left(R_{2j}^{1+\alpha_{B,j}} - R_{2j+1}^{1+\alpha_{B,j}}\right)$$
$$+ Z_{B,i}\left(R_{2i}^{1+\alpha_{B,i}} - r^{1+\alpha_{B,i}}\right) \tag{13}$$

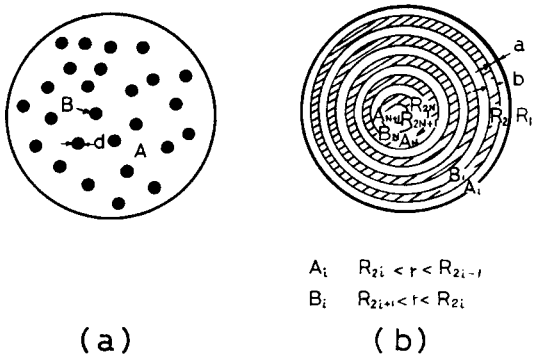

Fig. 9. Dispersoid-matrix model and concentric multilayer model.

respectively, where

$$Z_{A,i} = \frac{1}{1+\alpha_{A,i}}\left(\frac{\zeta}{2K_{A,i}}\right)^{\alpha_{A,i}} \tag{14}$$

$$Z_{B,i} = \frac{1}{1+\alpha_{B,i}}\left(\frac{\zeta}{2K_{B,i}}\right)^{\alpha_{B,i}} \tag{15}$$

$$\zeta = \frac{\partial P}{\partial Z} \tag{16}$$

$$\alpha_A = 1/n_A, \qquad \alpha_B = 1/n_B \tag{17}$$

The boundary conditions are

$$\text{at } r = R_1; \qquad V_{A,i} = 0$$

$$\text{at } r = R_{2i}; \qquad V_{A,i} = V_{B,i}$$

$$\text{at } r = R_{2i+1}; \qquad V_{A,i+1} = V_{B,i}$$

The volumetric flow rates $Q_{A,i}$ and $Q_{B,i}$ are obtained by

$$\begin{aligned} Q_{A,i} &= \int_{R_{2i}}^{R_{2i-1}} V_{A,i} \cdot 2\pi r\, dr \qquad (i = 1 \sim N+1) \\ &= 2\Pi\left[-\frac{Z_{A,i}}{3+\alpha_{A,i}}\left(R_{2i-1}^{3+\alpha_{A,i}} - R_{2i}^{3+\alpha_{A,i}}\right) + \frac{1}{2}\left(R_{2i-1}^2 - R_{2i}^2\right)\right. \\ &\quad \times\left\{\sum_{j=1}^{i-1} Z_{A,j}\left(R_{2j-1}^{1+\alpha_{A,j}} - R_{2j}^{1+\alpha_{A,j}}\right)\right. \\ &\quad \left.\left. + Z_{A,i}R_{2i-1}^{1+\alpha_{A,i}} + \sum_{j=1}^{i-1} Z_{B,j}\left(R_{2j}^{1+\alpha_{B,j}} - R_{2j+1}^{1+\alpha_{B,j}}\right)\right\}\right] \end{aligned} \tag{18}$$

$$\begin{aligned} Q_{B,i} &= \int_{R_{2i+1}}^{R_{2i}} V_{B,i} \cdot 2\pi r\, dr \qquad (i = 1 \sim N) \\ &= 2\pi\left[-\frac{Z_{B,i}}{3+\alpha_{B,i}}\left(R_{2i}^{3+\alpha_{B,i}} - R_{2i+1}^{3+\alpha_{B,i}}\right) + \frac{1}{2}\left(R_{2i}^2 - R_{2i+1}^2\right)\right. \\ &\quad \times\left\{\sum_{j=1}^{i} Z_{A,i}\left(R_{2j-1}^{1+\alpha_{A,j}} - R_{2j}^{1+\alpha_{A,j}}\right)\right. \\ &\quad \left.\left. + \sum_{j=1}^{i-1} Z_{B,j}\left(R_{2j}^{1+\alpha_{B,j}} - R_{2j+1}^{1+\alpha_{B,j}}\right) + Z_{B,i}R_{2i}^{1+\alpha_{B,i}}\right\}\right] \end{aligned} \tag{19}$$

The total volumetric flow rate in capillary is

$$Q = \sum_{i=1}^{N+1} Q_{A,i} + \sum_{i=1}^{N} Q_{B,i} \tag{20}$$

The apparent shear rate and the apparent viscosity are obtained using ζ and Q as follows.

$$\dot{\gamma}_a = \frac{4Q}{\pi R_1^3} \tag{21}$$

$$\eta_a = \frac{\pi R_1^4}{8Q}\zeta \tag{22}$$

The apparent viscosity, apparent shear rate, as well as those of each component all cannot be given analytically. Then the equations given in (12)–(22) must be calculated numerically. For that, the viscosity-shear rate curve of each parent component (PC and SAN) must be given. The curve was given by applying Rabinowitsch correction[8] to the measured apparent viscosity-shear rate curve of each component. In applying the correction, the treatment of the jump at the end of the second Newtonian region of SAN is a little confusing. The correction was made separately to the apparent curve below the shear rate at which the jump takes place and to the curve above the shear rate, and the two corrected curves were connected with discontinuity, in which the discontinuity was made the same as that in the apparent curve. The corrected results are given in Table I, by approximating the result by power laws.

The apparent viscosity of the binary system calculated by using the equations, in which the viscosity is approximated by the power law given in the table, is plotted by solid lines against the apparent shear rate in Figure 10. The calculated curves are approximately in good agreement with the mea-

TABLE I
Power-Law Approximation of $\eta \sim \dot{\gamma}$ Relationship
for Each Component (Corrected by Rabinowitsch Method)

Component	Power-law approximation	
A (PC)	$\tau = 3.32 \times 10^4\ \dot{\gamma}^{0.37}$	(Pa)
	$\eta = 3.32 \times 10^4 \dot{\gamma}^{-0.63}$	(Pa.s)
B (SAN)	(i) $\dot{\gamma} \leq \dot{\gamma}_{c1}$	
	$\tau = 3.80 \times 10^3 \gamma^{0.43}$	(Pa)
	$\eta = 3.80 \times 10^3 \dot{\gamma}^{-0.57}$	(Pa.s)
	(ii) $\dot{\gamma}_{c1} \leq \dot{\gamma} \leq \dot{\gamma}_{c2}$	
	$\tau = 9.30 \times 10^{-1} \dot{\gamma}$	(Pa)
	$\eta = 9.30 \times 10^{-1}$	(Pa.s.)
	(iii) $\dot{\gamma}_{c2} < \dot{\gamma}$	
	$\tau = 2.95 \times 10^5 \dot{\gamma}^{0.2}$	(Pa)
	$\eta = 2.95 \times 10^5 \dot{\gamma}^{-0.8}$	(Pa.s)
	$\dot{\gamma}_{c1} = 2.7 \times 10^6\ (s^{-1})$	
	$\dot{\gamma}_{c2} = 4.1 \times 10^6\ (s^{-1})$	

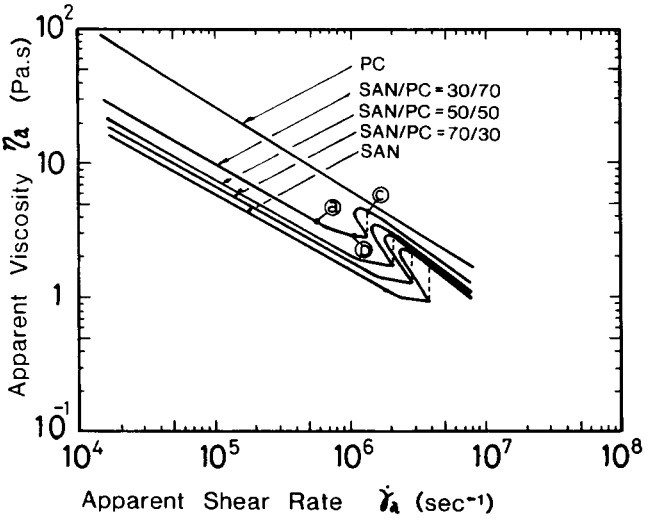

Fig. 10. Apparent viscosity vs. apparent shear rate curves calculated by using concentric multilayer model.

sured ones (shown Fig. 2), with the exception of the presence of backward movement in the calculated curves at the end of the plateau region. The rather good agreement between the calculation and experiment proves the assumption and the concentric multilayer model valid.

The presence of the plateau region at the lower shear rate for the binary systems than that for the parent macromolecule, SAN, is explained as follows:

In any flowing binary system, the shear rate of the lower viscosity component is higher than that of the higher viscosity one. The difference in the shear rates depend on the viscosity of each parent component, composition of the binary system and flow rate.

Calculated shear rate as a function of radial distance in the capillary are shown for SAN 30%–PC 70% system in Figures 11, 12, and 13, respectively, for the shear rate of 4.42×10^5 s^{-1}, 1.06×10^6 S^{-1}, and 1.25×10^6 s^{-1}, for example.

The shear rates of the value of 4.42×10^5 s^{-1}, 1.06×10^6 s^{-1}, and 1.25×10^6 s^{-1} correspond to the points indicated as a, b, and c on the curve of SAN 30%–PC 70% in Figure 10.

The shear rate of the lower viscosity component SAN is about 1.5 order higher than that of the higher viscosity component PC at any shear rate.

Therefore, as shown in the examples, the shear rate of some parts of the lower viscosity component, SAN, exceeds or equals the apparent shear rate, and the shear rate of the higher viscosity component, PC, is smaller than the apparent one. The higher shear rate occurs near the capillary wall. The apparent viscosity of the binary system is given by weighted mean of those of the components. The weight is given in equations (12)–(22). At some apparent shear rate, which is lower than the shear rate of the beginning of the plateau region of SAN, the shear rate of SAN component in binary system comes to represent the shear rate of the beginning of the plateau region of SAN. The apparent viscosity of the binary system shows a point of inflection under the

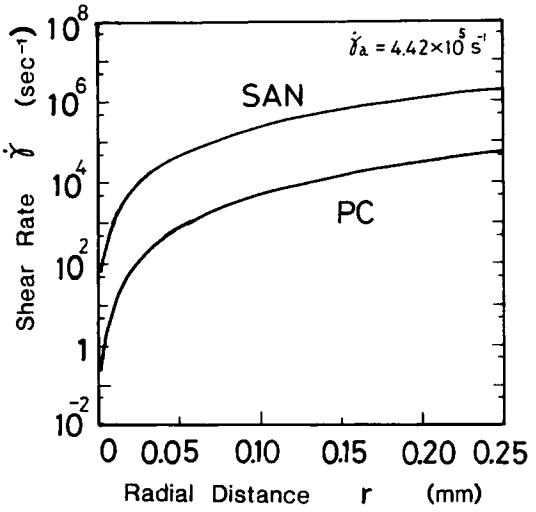

Fig. 11. Calculated shear rate as a function of radial distance in the capillary for SAN 30%–PC 70% system (apparent shear rate: $\dot{\gamma}_a = 4.42 \times 10^5\ s^{-1}$).

influence of the constant viscosity in the plateau region SAN. This explains the shift of the beginning point of the plateau region to the lower shear rate in the binary system.

As pointed out in this explanation, in a binary system in which a singular point appears in one of the $\eta \sim \dot{\gamma}$ curves of the parent materials, the singularity occurs at lower shear rate or higher shear rate than that in the parents' singularity depending on the viscosity of the parent having the singularity. If the viscosity of the parent is lower than the other, the singularity in the binary system occurs at lower shear rate, and vice versa.

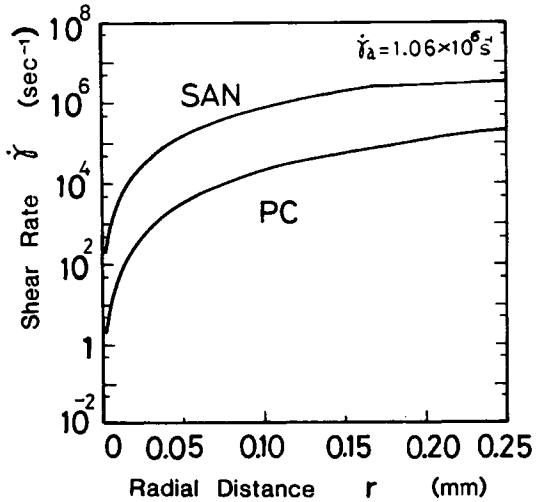

Fig. 12. Calculated shear rate as a function of radial distance in the capillary for SAN 30%–PC 70% system (apparent shear rate: $\dot{\gamma}_a = 1.06 \times 10^6\ s^{-1}$).

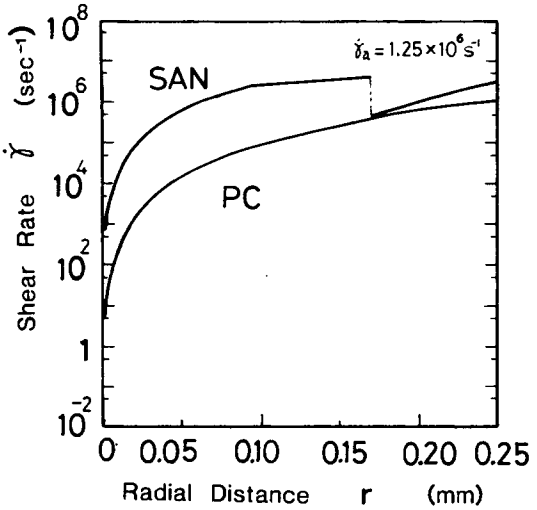

Fig. 13. Calculated shear rate as a function of radial distance in the capillary for SAN 30%–PC 70% system (apparent shear rate: $\dot{\gamma}_a = 1.25 \times 10^6\ s^{-1}$).

The end point of the plateau corresponding to that of SAN shifts to lower shear rate in the same way. The apparent plateau region in the binary system, however, does not strictly have a constant value, or it is not a strict plateau, as it is a weighted mean and it varies more or less under the influence of the decreasing viscosity of PC. This explains the presence of the pseudo plateau region in the binary system, mentioned in regard to the experimental results.

The backward motion in the calculated viscosity-shear rate curve resulted from the viscosity jump in the curve of SAN at the end of the plateau region. This is explained as follows; The apparent viscosity is given from some combination of those of each parent component as shown in eqs. (12)–(22). At the end of the plateau in the SAN curve, the viscosity of SAN jumps to the high value discontinuously, then the calculated apparent viscosity increases at the end of the pseudo plateau region of the binary system. The calculated apparent shear rate of the binary system is given by the combination of the shear rate of each layer. At the end of the pseudo plateau region of the binary system, the shear rate of some SAN layers located near the capillary wall reaches that of the end of the plateau region of SAN. There the viscosity of SAN jumps up to the high value, then the shear rate of the SAN layers jumps down to lower value (e.g., Fig. 10). As a result, the apparent shear rate goes down, making the backward motion in the calculated viscosity-shear rate curve of the binary system. The backward motion in the calculated viscosity in the viscosity-shear rate curve must take place in the single system, SAN, because in the nearest region to the capillary wall, the shear rate reaches first the end of the plateau. The flow there would then be unstable. This explains the instability of the measured viscosity of SAN. The backward motion, however, should not take place actually, because it is unstable and the apparent viscosity would jump up to the higher value at the end of the pseduo plateau region as shown by dotted line in Figure 10. The calculated apparent

viscosity-shear rate curve has a discontinuous increasing trend at the end of the region.

But the measured shear rate seems to lack this discontinuous increase in the binary system SAN 50%–PC 50%. This diminished discontinuity is not fully explained at present.

The calculated value in the shear rate above the pseudo plateau region agrees well with the measured one.

A more precise comparison of the calculated curve with the measured one reveals that the beginning as well as the end of the measured pseudo plateau region is slightly shifted to lower shear rate than the calculated one. This is thought to occur because the lower viscosity component has a tendency to locate nearer the capillary wall than does the higher viscosity one.[7] The actual shear rate of the SAN layer must be much more advanced than the calculated one, assuming the uniform distribution of each component layer. This explains the lower shear rate of the measured pseudo plateau region than that of the calculated one.

CONCLUSION

Extremely high shear rate processing was applied to the compound system of SAN/PC. The viscosity was measured against the shear rate up to 10^7 s^{-1}.

The first non-Newtonian region, second Newtonian region, and second non-Newtonian region take place in the compound system in a very similar way to those in the parent polymers, SAN and PC.

For the calculation of the viscosity-shear rate curve, a concentric multilayer model was proposed. It gives good agreement between the calculated and the measured values.

A new mechanism for the occurrence of the non-Newtonian, second Newtonian, and second non-Newtonian regions was proposed. The occurrence of the first non-Newtonian region is considered to be attributed to the decrease of entanglement density. As the shear rate is increased further, the macromolecules are stretched nearly to their full length at least near the capillary wall. Therefore, the rate of disentanglement against the increase of shear rate becomes very small—the plateau takes place. Moreover, the stretched macromolecules begin to snap. The recoiling of the snapped macromolecules creates new entanglement. The abrupt increase in the viscosity at the end of the plateau region occurs due to the superiority of the increase of viscosity through the creation of new entanglement due to the decrease of the molecular weight. As the shear rate is further increased, the entangled macromolecules are more frequently disentangled by the increased shear flow and snapping of the stretched macromolecules. This accounts for the occurrence of second non-Newtonian region.

Nuclear spin–spin relaxation time measurements on SAN exposed to the high shear proved the proposed explanation.

The authors express their thanks to Mr. A. Koiwai for his assistance with the numerical calculation work and to Mr. T. Okamoto and Mr. T. Ohmori for their assistance with some of the experimental work.

They also thank Dr. M. Kurata, Dr. H. Odani, Dr. K. Osaki, and Dr. N. Nemoto of the Institute for Chemical Research of Kyoto University for helpful discussion throughout the work.

References

1. H. Takahashi, T. Matsuoka, and T. Kurauchi, *J. Appl. Polym. Sci.*, **30**, 4669 (1985).
2. A. Charlesby, R. Folland, and J. H. Steven, *Proc. R. Soc., Lond.*, **A.355**, 189 (1977).
3. S. Kaufman, W. P. Slichter, and D. D. Davis, *J. Polym. Sci. A-2*, **9**, 829 (1971).
4. D. Soong and M. Shen, *Polym. Eng. Sci.*, **20**, 1177 (1980).
5. R. Folland and A. Charlesby, *Polymer*, **20**, 207 (1979).
6. C. C. Lin, *Polym. J.*, **11**, 185 (1979).
7. C. D. Han and H. B. Chin, *Polym. Eng. Sci.*, **19**, 1156 (1979).
8. B. Rabinowitsch, *Z. Physik. Chem.*, **A145**, 1 (1929).

Received September 30, 1987
Accepted April 21, 1988